# Supporting Information

## Hedstrom et al. 10.1073/pnas.1308889111

### SI Materials and Methods

**Animals.** Transgenic mouse lines used as previously described (1, 2). The hot-plate test was performed using hot-plate analgesia meters; Columbus Instruments for Fig. 1 *A* and *B*; IITC for Fig. 2 *A* and *B* and Fig. S4. Paw withdrawal latency was measured as the time required for the mouse to visibly respond to the thermal stimulus, e.g., licking paws, shaking hindpaws, or jumping. Mechanical sensitivity was tested by simulation of the plantar surface of the hindpaw with a series of von Frey filaments. The threshold was determined as the lowest force that evoked a visible withdrawal response. The use of animals was approved by the Animal Care and Use Committee of Boston Children's Hospital.

**Diabetic Neuropathy.** Adult female C57BL/6J mice were made diabetic (blood glucose, >15 mmol/L) by injection of streptozotocin (STZ) (90 mg/kg, i.p.) on 2 consecutive days, with confirmation of hyperglycemia made 7 d after STZ delivery. Paw thermal response latency of the right paw was measured every 2 wk from weeks 8–16 of diabetes using a modified Hargreaves test, as described (3).

**Preparation and Use of XIB4035.** The cream containing XIB4035 (1.5 mM; ZereneX Molecular) consisted of *N*-methyl-pyrrolidone (6.25%), isopropyl myristate (6.25%), and petroleum jelly (87.5%). Control cream had the same ingredients without XIB4035. Cream was applied twice daily to the hindpaws of mice for lengths of time indicated.

**Plastic Embedding and Electron Microscopy.** Tissue was prepared as in ref. 1. Photographs were taken using the Tecnai G2 Spirit BioTWIN transmission electron microscope.

**Tissue Collection and Immunostaining.** Mice were anesthetized with 2.5% Avertin. For experiments involving line-D mice, hindpaws were removed, immersion fixed in 2% paraformaldehyde, 14% picric acid in 0.1 M phosphate buffer (pH 7.4) overnight at 4 °C, and cryoprotected in 20% sucrose overnight at 4 °C. Footpad skin was dissected from hindpaws, embedded in OCT, sectioned at 30 μm, and stained as floating sections with protein gene product 9.5 (PGP9.5) rabbit polyclonal antibody (Ultraclone; 1:1,000) overnight at 4 °C followed by incubation with goat anti-rabbit Alexa 488 (Invitrogen) at 1:1,000 for 1 h at room temperature. For experiments involving diabetic mice, hindpaws were removed and fixed for 24 h in 4% paraformaldehyde in 0.1 M phosphate buffer. Samples were embedded in paraffin and cut at a thickness of 6 μm. Sections were collected onto glass slides and incubated with an antibody against the panneuronal marker PGP9.5 and developed for HRP reaction (1:1,000; Biogenesis) (4).

Spinal cords were collected from mice anesthetized with 2.5% Avertin, immersion fixed in 4% paraformaldehyde in 0.1 M phosphate buffer (pH 7.4) for 2 h at 4 °C, and cryoprotected in 20% sucrose overnight at 4 °C. Tissue was embedded in OCT, sectioned at 15 μm, and stained, mounted on slides, and incubated with TrpV1 rabbit polyclonal antibody (Abcam; 1:2,000) and Alexa 488-conjugated isolectin-B4 overnight at 4 °C followed by incubation with goat anti-rabbit Alexa 594 (Invitrogen) at 1:1,000 for 1 h at room temperature. In all experiments, nuclei were stained with DAPI during secondary antibody incubations.

**Immunostaining Analysis.** For experiments involving line-D mice, skin section images were acquired as 30-μm *Z* stacks (1-μm intervals) and processed as maximum-intensity projections using a Zeiss LSM 700 microscope and ZEN software. Acquisition measures were set using control-treated wild-type sections and used for all sections imaged. A measured line was drawn using the DAPI channel to delineate the border between basal keratinocytes and outer layers of the epidermis. All PGP9.5-positive intraepidermal nerve fibers (IENFs) crossing the border were counted and expressed as a number per 100-μm length. For experiments involving diabetic mice, the total numbers of IENFs were counted blinded to group identity. The length and area of each section were determined using point-counting methods and a grid reticle containing 100 squares, each 25 $\mu m^2$. The number of intersections between the stratum granulosum and the grid lines were counted and length calculated using a previously derived equation (4). Analysis of IENF density was blinded to genotype and treatment.

Spinal cord images were acquired using a Zeiss Axioscope microscope. Exposure times for each channel were set using wild-type control-treated sections and used for all images. Analysis of the presence of dorsal horn isolectin-B4 (IB4) staining was blinded to genotype and treatment.

**Promoter Cloning and Stable Cell Generation.** The tyrosine hydroxylase (TH) promoter was cloned into the pGL3 basic vector (Promega), as previously described (5) (TH-pGL3). Briefly, a 2-kb promoter region upstream from the transcription initiation site of the rat *TH* gene was cloned from genomic DNA using the primer sequences TGACGCGTAGGCACAGCTCCCTCCTACCCCGT and AGAAGCTTCCCTCGCCAGGCAGGCGCCCTCT. SH-SY5Y cells were cotransfected with the TH-pGL3 and the pBabe-puromycin expression vectors at a molar ratio of 10:1.

**Cell Assays.** SH-SY5Y-THpGL3 cells were maintained in DMEM/F12, 5% FBS, and 1% penicillin/streptomycin on collagen-coated plates (4 μg/mL). Neuro-2A cells were grown in MEM, 5% FBS, and 1% penicillin/streptomycin. BE(2)-C cells were grown in DMEM/F12 media containing 5% FBS and 1% penicillin/streptomycin. PC-12 cells were maintained in media containing RPMI 1640, 10% horse serum, 5% FBS, and 1% penicillin/streptomycin on collagen-coated plates. For luciferase assays, cells were treated for either 10 min with washout or overnight with various molecules and assayed for firefly luciferase 16–24 h post-treatment initiation using the luciferase assay system (Promega).

For phosphorylated Ret immunoblot experiments, cells were treated with various combinations of molecules for 10 min and either collected immediately or had treatment washed out and returned to control treatment media for the times indicated before cell collection. Lysates were collected in lysis buffer containing the following: 1% TX-100, 0.25% deoxycholic acid, 0.1 mM sodium fluoride, 0.1 mM sodium pyrophosphate, 0.02 mM sodium orthovanadate, and protease inhibitors. Immunoblots were blocked in 5% BSA in TBST plus 0.1 mM sodium fluoride, 0.1 mM sodium pyrophosphate, and 0.02 mM sodium orthovanadate, and probed in blocking solution using anti-phosphotyrosine (4G10) mouse monoclonal antibody (1:4,000; EMD Millipore). Secondary detection was performed in blocking solution using HRP-conjugated goat anti-mouse antibodies (1:1,000; MP Biomedicals).

N2A cells were transfected with expression plasmids expressing a membrane bound form of EGFP (mGFP), rat GFRα1, or human GFRα3 (GFRα constructs were kind gifts from Dr. Jefferey Milbrandt at Washington University School of Medicine, St. Louis, MO). N2A and PC-12 cells were starved in basal media containing 1% FBS overnight before treatments. Glial

cell line-derived neurotrophic factor (GDNF), neurturin (NRTN), and artemin (ARTN) were purchased from PeproTech. β-NGF (R&D Systems) at 50 μg/mL was used to stimulate TrkA receptor phosphorylation in PC-12 cells.

**Immunoblot Quantification.** Blots were imaged using an Image Quant LAS4000 mini (GE Healthcare Life Sciences). Densitometry was performed using ImageJ software over four individual experiments. Mean pixel intensity was measured over the GDNF-stimulated band at 0 min. All other phosphorylated RET bands within an experiment were measured using the identical area selection. Blot background was measured and subtracted from all values within each experiment before normalization. All measurements were normalized to the average mean pixel intensity of their respective GDNF-stimulated band at 0 min. Average normalized mean pixel intensity was calculated and plotted. Statistical significance was determined between untreated, GDNF alone, and GDNF plus 20 μM XIB4035 within each time point.

**Statistical Analyses.** All statistical analyses are as indicated and were performed using Prism 4 (GraphPad Software). SEM was used to indicate error in all analyses as $n \geq 3$. For Fig. 3*C*, comparison of the nonlinear curve regression was performed using an $F$ test. Analysis of the minimal ligand dose necessary to induce luciferase activity (Fig. 3*C*) was performed by Student $t$ test comparing the average fold luciferase induction from three experiments to control (nontreated).


1. Chen S, et al. (2003) Disruption of ErbB receptor signaling in adult non-myelinating Schwann cells causes progressive sensory loss. *Nat Neurosci* 6(11):1186–1193.
2. Zwick M, et al. (2002) Glial cell line-derived neurotrophic factor is a survival factor for isolectin B4-positive, but not vanilloid receptor 1-positive, neurons in the mouse. *J Neurosci* 22(10):4057–4065.
3. Beiswenger KK, Calcutt NA, Mizisin AP (2008) Dissociation of thermal hypoalgesia and epidermal denervation in streptozotocin-diabetic mice. *Neurosci Lett* 442(3):267–272.
4. Beiswenger KK, Calcutt NA, Mizisin AP (2008) Epidermal nerve fiber quantification in the assessment of diabetic neuropathy. *Acta Histochem* 110(5):351–362.
5. Xiao H, Hirata Y, Isobe K, Kiuchi K (2002) Glial cell line-derived neurotrophic factor up-regulates the expression of tyrosine hydroxylase gene in human neuroblastoma cell lines. *J Neurochem* 82(4):801–808.


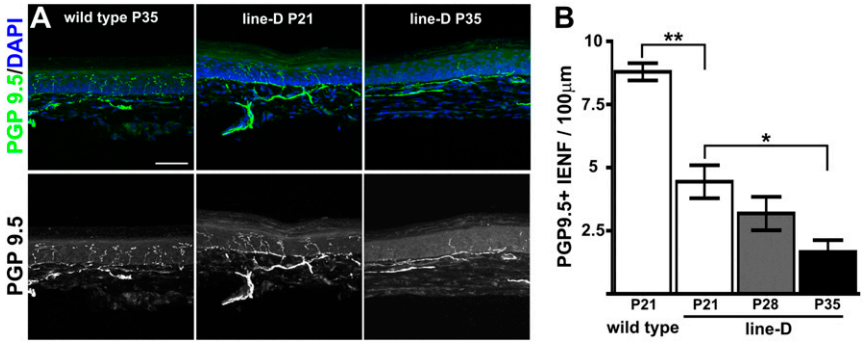


**Fig. S1.** IENF density loss in line-D mice correlates with deteriorating thermonociception. (*A*) Immunolabeling of PGP9.5-positive nerve terminals demonstrates a loss of IENFs in footpads of line-D mutant mice between P21 and P35. Nuclei are stained with DAPI. (Scale bar: 100 μm.) (*B*) Quantification of nerve terminals in the footpad skin of wild-type mice at P21 and line-D mice at P21, P28, and P35 shows that line-D mice have IENF loss already by P21, which worsens with age concurrent with declining sensory function (wild-type P21 vs. line-D P21, $t$ test, $^{**}P < 0.01$; line-D P21, P28, and P35, ANOVA Newman–Keuls post hoc, $n = 4$; $^{*}P < 0.05$; error bars indicate SEM).

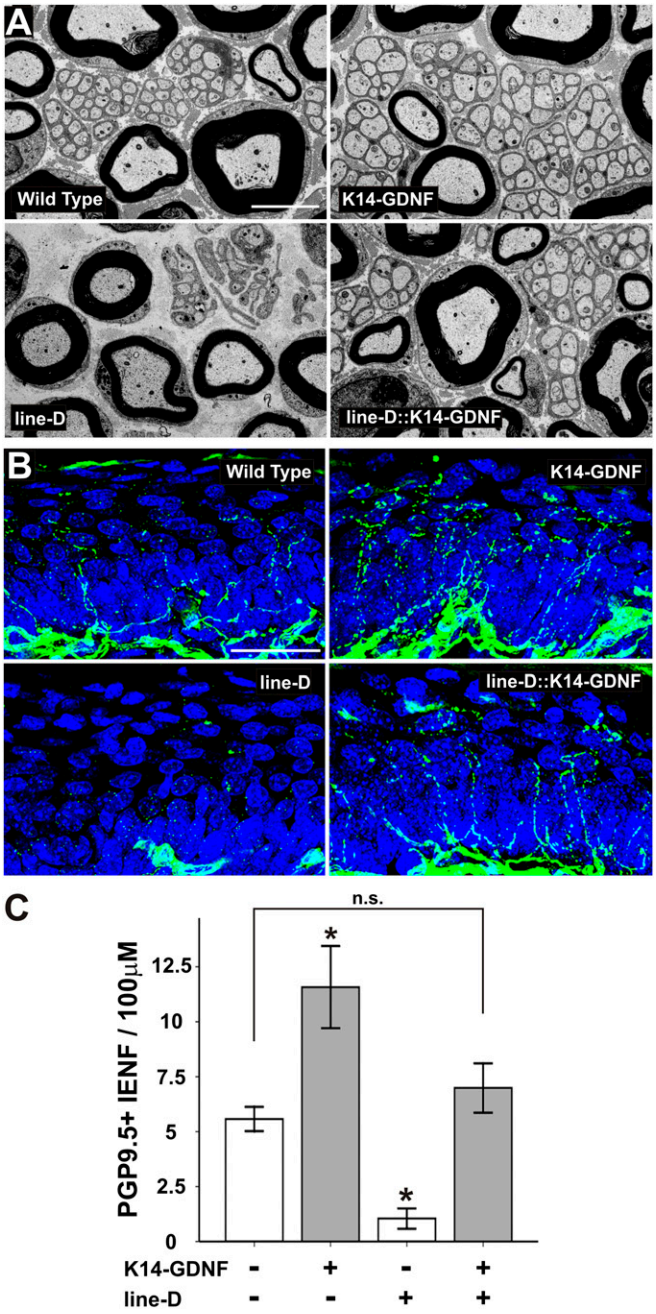


**Fig. S2.** Overexpression of GDNF in the skin rescues the small-fiber pathology of line-D mice. (*A*) Electron micrographs of transverse sections from sciatic nerves show that Remak bundle structure is lost in line-D mice but preserved in line-D::K14-GDNF mice at P30. (Scale bar: 4 μm.) (*B*) The density of PGP9.5-positive nerve terminals in footpads at P30 is increased by GDNF overexpression (K14-GDNF) and reduced in line-D mice compared with double-transgenic mice. Skin innervation in K14-GDNF::line-D mice is not different from in wild types. (Scale bar: 25 μm.) (*C*) IENF density is maintained in line-D mice by GDNF skin overexpression. Quantification of nerve terminals in footpad skin of line-D::K14-GDNF mutants at P30 show that GDNF overexpression maintains IENF density at wild-type levels (one-way ANOVA with Newman–Keuls post hoc test, $n = 3$; depicted significance vs. wild type; n.s., not statistically significant; $^*P < 0.05$; other comparisons: line-D vs. line-D::K14-GDNF and K14-GDNF vs. line-D::K14-GDNF, $P < 0.05$; K14-GDNF vs. line-D, $P < 0.001$; error bars indicate SEM).

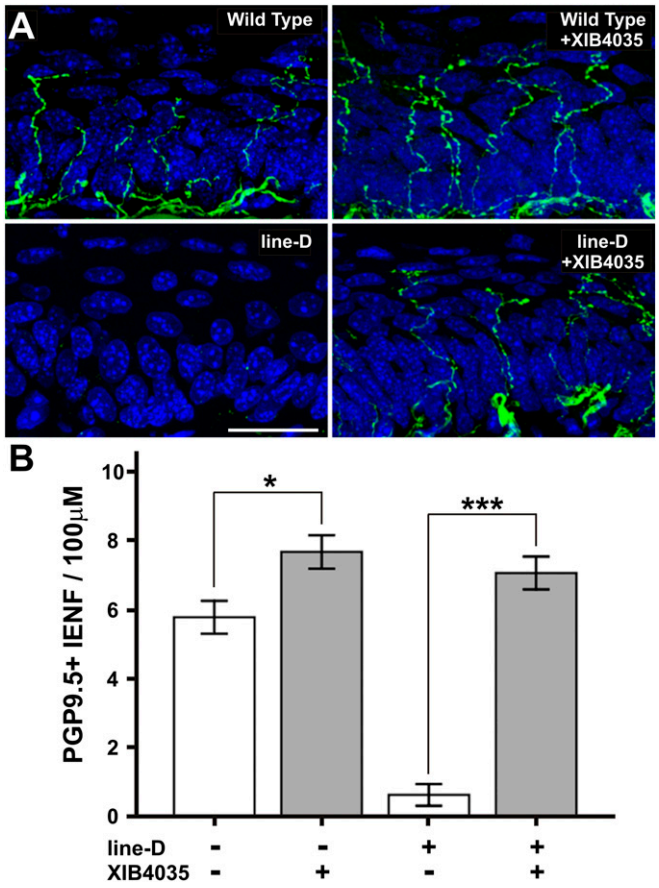


**Fig. S3.** Treatment of line-D mice with XIB4035 during early SFN progression prevents IENF loss in the skin. (*A*) The number of PGP9.5-positive nerve terminals in footpads is increased after 4 wk of treatment with XIB4035. The fiber loss seen in line-D mice treated with control cream is prevented by XIB4035 treatment. (Scale bar: 25 μm.) (*B*) Quantification of nerve terminals in the footpad skin after 4 wk of treatment (P49) shows that the number of PGP9.5-positive endings in both wild type and line-D treated with XIB4035 is greater than vehicle-treated animals of the same genotype (one-way ANOVA with Newman–Keuls post hoc test, $n = 5$; $^{*}P < 0.05$; $^{***}P < 0.001$; other comparisons, WT +vehicle vs. line-D +XIB4035 and WT +XIB4035 vs. line-D +XIB4035, not statistically significant; WT +vehicle vs. line-D +vehicle and WT +XIB4035 vs. line-D +vehicle, $P < 0.001$; error bars indicate SEM).

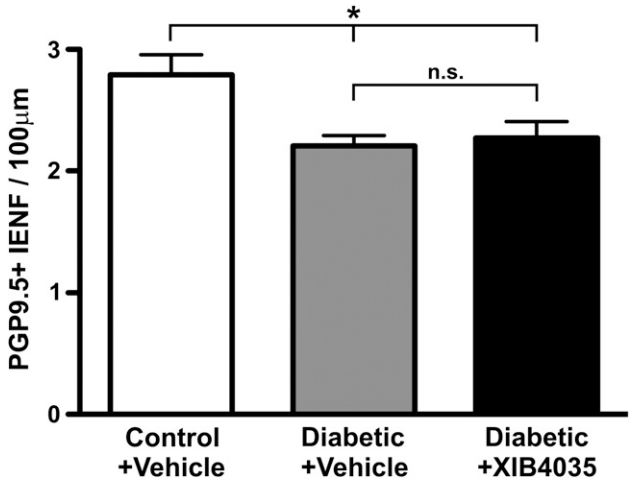


**Fig. S4.** XIB4035 treatment of diabetic mice does not rescue IENF loss. Quantification of IENF density in footpad skin shows that diabetes leads to IENF loss that is not altered by XIB4035 treatment (one-way ANOVA with Newman–Keuls post hoc test, $n \geq 6$; n.s., not statistically significant; $^{*}P < 0.05$; error bars indicate SEM).

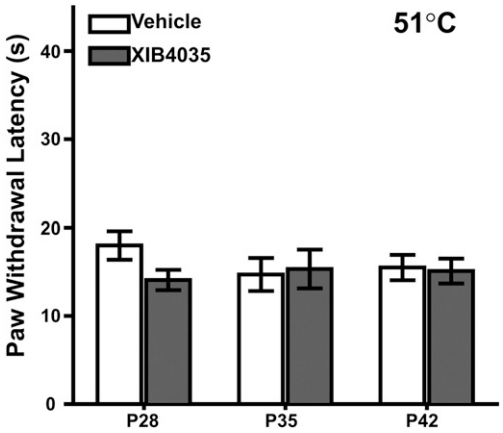


**Fig. S5.** XIB4035 does not alter thermal nociceptive function in wild-type mice. Wild-type mice treated with XIB4035 beginning at 4 wk of age (P28) and continuing to 6 wk of age (P42) showed no hypersensitivity to a milder noxious thermal stimulus (51 °C) than the one used in all other hot-plate testing (54 °C) [Student *t* test, $n \geq 10$; P28 ($P = 0.0671$), P35 ($P = 0.8343$, P42 ($P = 0.8492$); error bars indicate SEM].

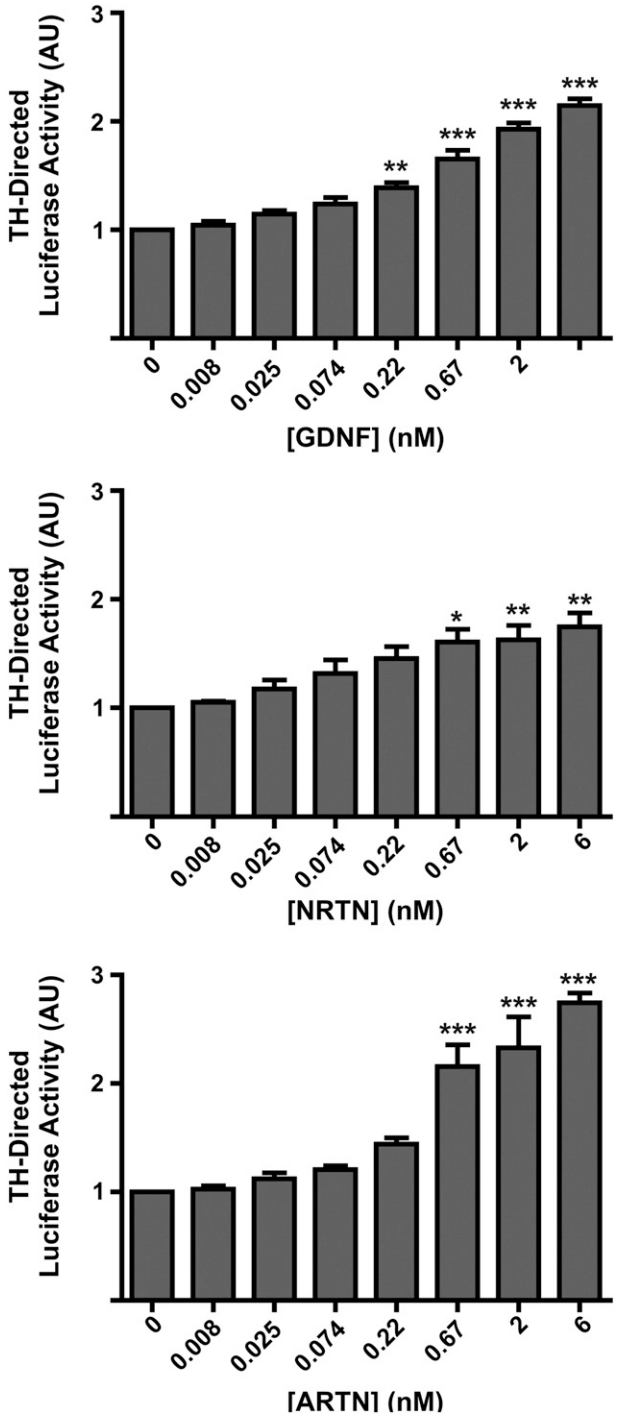


**Fig. S6.** GDNF-family ligands induce activation of the TH promoter luciferase reporter in a dose-dependent fashion. SH-SY5Y human neuroblastoma cells carrying a TH-luciferase reporter (SH-SY5Y-THpGL3) show dose-dependent luciferase activity responses to various ligand (GDNF, NRTN, or ARTN) concentrations (one-way ANOVA Newman–Keuls post hoc test, $n = 3$; vs. control, $^{*}P < 0.05$, $^{**}P < 0.01$, $^{***}P < 0.001$; error bars indicate SEM).

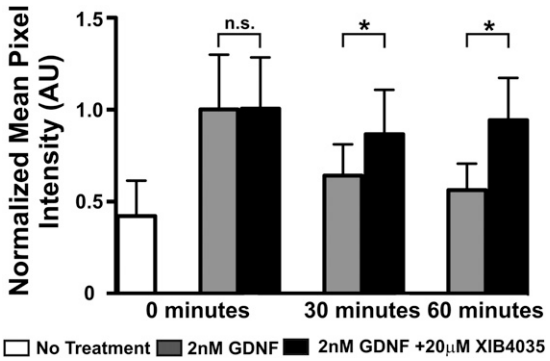


**Fig. S7.** Cotreatment with XIB4035 prolongs ligand-induced RET phosphorylation. Quantification of RET tyrosine phosphorylation levels by Western blot shows that cotreatment with XIB4035 does not alter the level of RET phosphorylation induced by 10-min treatment by GDNF (0 min), but prolongs RET phosphorylation after treatment is washed out. One-way ANOVA with Newman–Keuls post hoc test; $n = 4$ independent experiments. ANOVAs were calculated for each time point together with the untreated sample. p-RET levels in the untreated samples are not different from that in the 30- and 60-min GDNF treatment alone. n.s., not statistically significant; $*P < 0.05$; error bars indicate SEM.

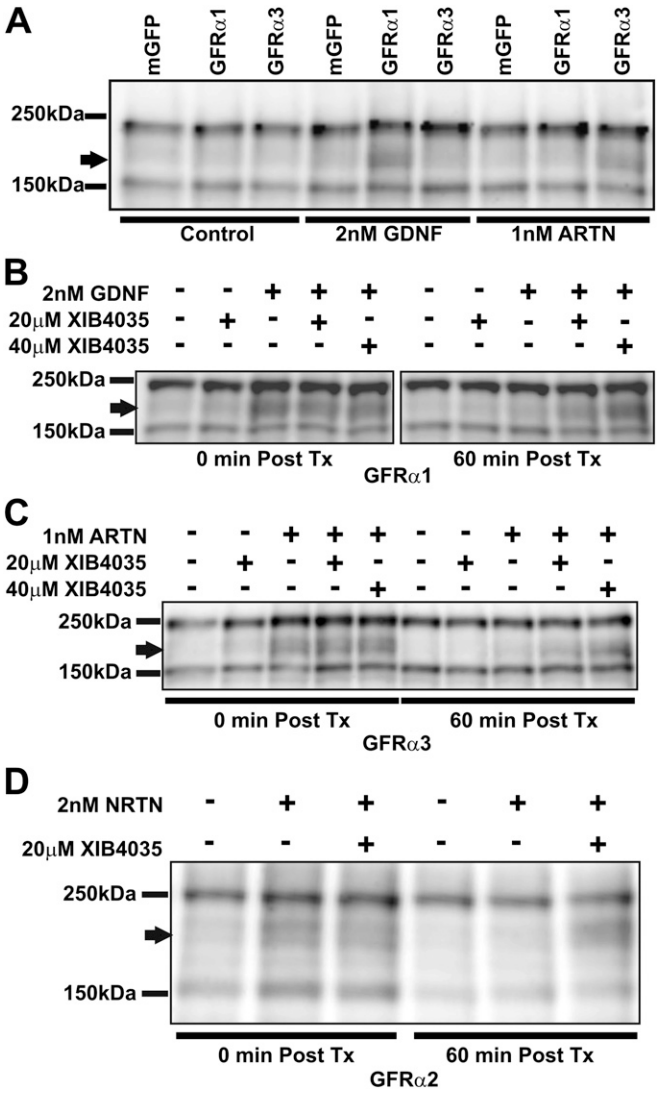


**Fig. S8.** XIB4035 prolongs RET phosphorylation in cells expressing either GFRα1, 2, or 3 upon stimulation with cognate ligands. (*A*) Control N2A cells (transfected with mGFP construct) lack RET activation upon stimulation with GFLs. Transfection with GFRα1 or GFRα3 confers ligand-induced RET activation to N2A cells and demonstrates ligand/receptor pair specificity (GFRα1/GDNF or GFRα3/ARTN). (*B* and *C*) XIB4035 prolongs ligand-induced RET phosphorylation in either GFRα1 (*B*)- or GFRα3 (*C*)-expressing cells. RET phosphorylation in GDNF (*B*)- or ARTN (*C*)-treated samples returns to baseline by 60 min, whereas addition of 40 μM XIB4035 prolongs the ligand-induced RET phosphorylation to at least 60 min. (*D*) XIB4035 prolongs ligand-induced RET phosphorylation in GFRα2-expressing cells. RET phosphorylation in NRTN-treated samples returns to baseline by 60 min, whereas addition of 20 μM XIB4035 prolongs the ligand-induced RET phosphorylation to at least 60 min.

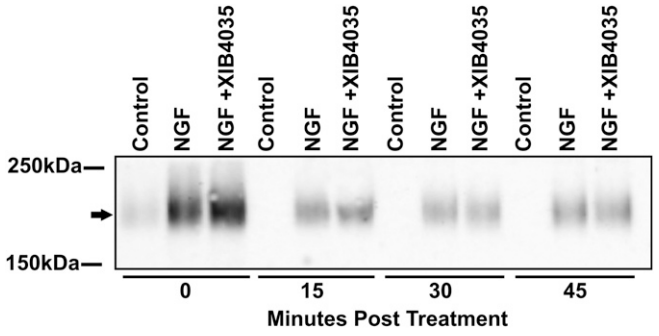


**Fig. S9.** XIB4035 does not change NGF-induced TrkA phosphorylation. NGF-induced TrkA phosphorylation in PC12 cells is not prolonged by addition of XIB4035.